Failure mode transitions of corroded deep beams exposed to marine environment for long period

Wenjun Zhu [a], Raoul François [b,*], David Cleland [c], Dario Coronelli [d]

[a] Tunnel and Underground Engineering Research Center of Ministry of Education, School of Civil Engineering, Beijing Jiaotong University, Beijing 100044, China
[b] Université de Toulouse, UPS, INSA, LMDC (Laboratoire Matériaux et Durabilité des Constructions), Toulouse, France
[c] School of Planning, Architecture & Civil Engineering, Queen's University, Belfast, UK
[d] Politecnico di Milano, Dipartimento di Ingegneria Strutturale, Milano, Italy

Received 30 January 2015
Revised 31 March 2015
Accepted 1 April 2015

1. Introduction

The corrosion of reinforcement is considered as one of the dominant causes leading to the premature deterioration of reinforced concrete (RC) constructions [1]. Corrosion reduces the residual cross-section of the steel bars and usually results in the concrete cover cracking and even spalling. Moreover, the corrosion products decrease the bond and anchorage between the steel bars and the concrete [2,3]. As a result, the structural performance of the concrete elements, including the serviceability and ultimate capacity, can be reduced [4].

Considerable research on the influence of reinforcement corrosion on the flexural performance of RC beams has been conducted during the last three decades. Mangat et al. [5] investigated three degrees of reinforcement corrosion in RC beams and found that the corrosion reduced the residual bending performance of RC members significantly. Malumbela et al. [6] examined the mechanical behavior of the corroded beams and reached the conclusion that a maximum mass loss of reinforcement of 1% can reduce the load-bearing capacity of RC beams by 0.7%. Torres-Acosta et al. [7] concluded that pitting corrosion plays an important role in the reduction of the flexural response of corroded beams.

The shear response of corroded RC beams is also currently attracting increased attention all over the world [8]. Cairns [9] studied the shear capacity of RC beams in which different parts of the longitudinal reinforcement were corroded and suggested that the shear capacity of the corroded beams was increased when the reinforcement was exposed in all but the most lightly reinforced sections. Higgins et al. [10] investigated the impact of corrosion of stirrups on the shear capacity of RC beams and indicated that corrosion reduced shear capacity and, therefore, overall deformation of the corroded beams.

However, most of the corrosion studies reported have been accelerated by impressed current or addition of calcium chloride during casting [11]. Yuan et al. [12] found that such accelerated corrosion led to different patterns from those of natural or climatic corrosion. Therefore, experiments dealing with natural corrosion are important to improve our understanding and confirm the applicability of the results from accelerated corrosion tests.

François et al. [13] have been carrying out a long-term programme concerning the corrosion of concrete beams at Laboratoire Matériaux et Durabilité des Constructions (L.M.D.C.) in Toulouse, in south-west France. All the beams have been stored in a chloride environment under service load since 1984, which is considered to be close to the natural conditions affecting real

* Corresponding author.
E-mail address: raoul.francois@insa-toulouse.fr (R. François).

Nomenclature

A_{sres}	residual cross-section of the tension bars
A_{swi}	residual cross-section of the stirrup i
A	cross-section of steel bar
Σ	perimeter of the tension bar
θ	angle of the inclined compression strut with respect to the tension bars
l_i	lever arm with respect to the forces of the tensile bars and the stirrups T_i from the top node O
L_{anch}	anchorage length
f_{sui}	stress of the bar i
f	yield or ultimate strength of the tension bars
P	applied load in the mechanical test
T	tension force in the reinforcement
τ_u	peak bond strength
σ_{max}	anchorage strength of the tension bars
α	parameter of τ – slip curve
γ	coefficient of the reduced perimeter length between the residual concrete and reinforcement

structures. A series of research works have been performed on the corroded beams and published results include the deterioration of the flexural performance of the corroded beams [14], the cracking process [15] and the residual mechanical properties of the corroded bars [16].

Shear behavior of RC beams is complex and can rarely be entirely isolated from flexure. A common way to study shear effect is to use deep beams where the flexural behavior becomes less significant and thus the failure mode is less influenced by flexural cracking. Two corroded deep beams with a shear span to depth ratio (a/d) of 1.84 were tested in 2010 [17]. The results showed a change in failure mode for the corroded beams compared to that of uncorroded beams of the same age and same a/d ratio. It was decided to study both higher and lower a/d ratios in order to confirm and better understand these results.

2. Experimental program

This programme was set up in 1984 in Toulouse, France. The aim was to investigate the process of reinforcement corrosion and its influence on the mechanical performance of the RC beams. The whole programme involved 36 beams with dimensions 3000 mm × 280 mm × 150 mm. Another 36 beams were cast and stored in a non-corrosive environment to be used as control beams. The beams were divided into Group A and Group B according to the diameters of the bars and the depths of concrete cover. In each group, the beams were loaded at two levels by a three point loading system, with bending moments at mid-span of 13.5 kN m and 21.2 kN m respectively.

The beams studied in this paper belonged to Group B, i.e. the moment was 21.2 kN m. The beams were labelled as B2Cl2 and B2Cl3. The original length of the two corroded beams was 3000 mm. In order to study the performance of the short-span corroded beams, each beam was cut to produce beams shorter than 1200 mm. The detailed information about the beams and the corrosion conditions will be presented in the following sections.

2.1. Material composition and properties

The concrete and cement compositions are shown in Table 1. The coarse aggregate was gravel with a maximum diameter of 15 mm. The ratio of water to cement was designed to be 0.5. However, the water content was readjusted in the casting process in order to achieve a constant workability of 70 mm in the slump test.

The concrete used for the RC beams was made with ordinary Portland cement. The compressive strength was 45 MPa, measured in tests on 110 mm × 220 mm cylindrical specimens at 28 days. The porosity was about 15.2%. The nominal yield strength for the steel bars was 500 MPa.

2.2. Loading system and chloride exposure conditioning

All the beams were loaded in a three-point loading system by coupling a beam of Group A and a beam of Group B as shown in Fig. 1. The span of all the beams was 2800 mm in the loading process. The moment at mid-span was 21.2 kN m for B2Cl2 and B2Cl3. Two uncorroded beams, B2T2 and B2T3, were subjected to the same loading condition.

As shown in Fig. 1, once the beams were loaded, they were all transferred into a chloride-spraying environment with a salt fog of 35 g/L, which was similar to the salt concentration of sea water. The beams were always stored in the room. However, the fog-spraying was varied at different periods so as to accelerate the corrosion process of the RC beams. Detailed information about the spraying system and the status of the beams is included in

Table 1
Concrete composition.

Mix composition							
Rolled gravel (silica + limestone)					5/15 mm		1220 kg/m^3
Sand					0/5 mm		820 kg/m^3
Portland cement: OPC HP (high performance)							400 kg/m^3
Water							200 kg/m^3
Cement composition	SiO_2	Al_2O_3	Fe_2O_3	CaO	MgO	SO_3	Na_2O
Weight (%)	21.4	6.0	2.3	63.0	1.4	3.0	0.5

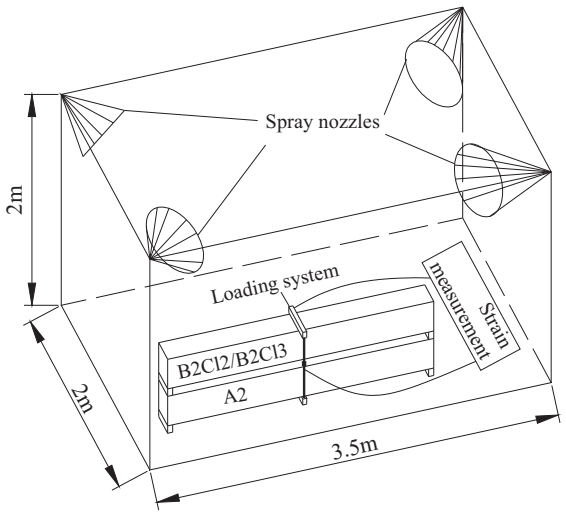

Fig. 1. Loading system and chloride environment.

Table 2
Wetting-drying cycles of the corroded beams.

Period (years)	Spraying state	Loading conditions	Conservation conditions	Temperature (°C)
0–6	Continuous spraying	Loaded	Confined room	About 20 °C
6–9	WDC	Loaded	Confined room	About 20 °C
9–19	WDC	Loaded	Confined room	CSWF
19–28	Stop spraying	Unloaded	Confined room	CSWF

* WDC: wetting-drying cycles (1 week of wetting and 1 week of drying).
* CSWF: climate of south-west France, with temperatures ranging from 5.1 to 21.3 °C average monthly value.

Table 2. The uncorroded beams were stored in the normal laboratory environment throughout the conditioning period.

2.3. Reinforced concrete specimens

The layout of the corroded beams and control beams is shown in Fig. 2. The deep beams were then cut from the original beams. The configuration of the deep beams cut from the B2Cl3 and B2T3 and their relationships with the original beams are shown in Fig. 2. The depth of concrete cover was 10 mm, which was the minimum value for beams in a non-aggressive environment at the time when the beams were cast. The current Eurocode 2 [18], specifies that the minimum cover depth required is 20 mm.

The original corroded beams B2Cl2 and B2Cl3 were tested at the age of 26 years in 2010 [13] and 28 years in 2012 [19] respectively to study the residual bending performance. Both beams failed by rupture of the tension bar in the middle zone. The cracks were also mainly distributed in the middle zone of the beams, and were assumed to have little influence on the mechanical performance of the two end portions. The deep beams, with maximum length of 1200 mm, were cut from the 3000-mm-long beams once the bending experiment had been conducted. The mechanical tests were subsequently carried out on the short beams in 2010 and 2012. The mechanical investigations were undertaken on uncorroded beams at the same time, which were cut after the bending tests. The four uncorroded short beams were named B2T2-1, B2T2-2, B2T3-1 and B2T3-2.

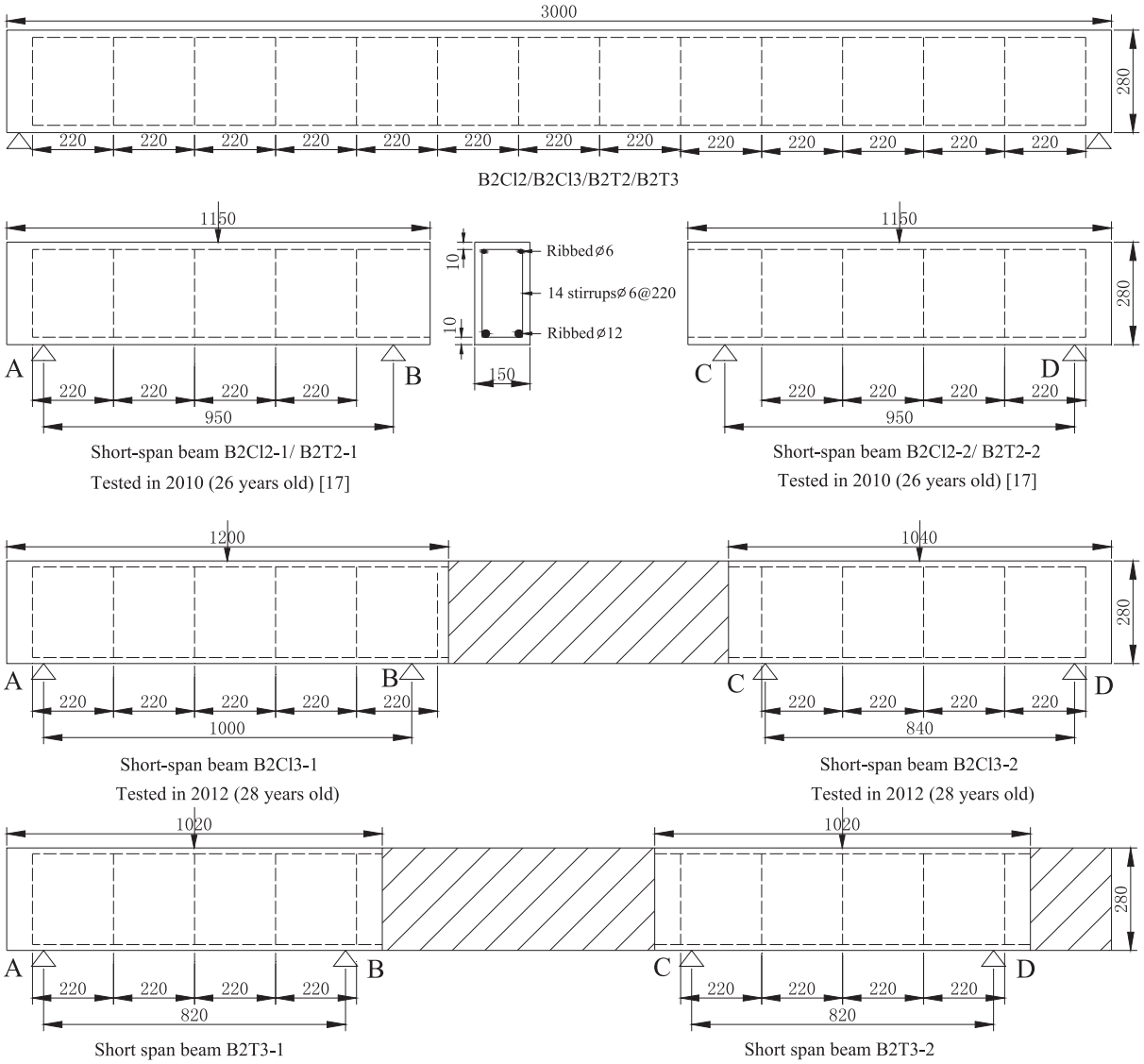

Fig. 2. Configurations of the deep beams analyzed in this paper.

3. Experimental results

Having been exposed to a corrosive environment for a long period, the beams were subjected to monotonic transverse loading to investigate their cracking status and residual mechanical performance. The deep beams were formed by sawing the original beams. The residual mechanical performance of the deep beams and the residual material properties of the tension bars extracted from the beams are studied in this section.

3.1. Description of the deep beams

When failure occurred in the original beams, the beams were cut into several parts. The original corroded beams B2Cl3 failed when the load was close to 40 kN, and the uncorroded beam B2T3 failed at a maximum load of 51 kN. The mechanical cracks and critical sections were mainly concentrated in the middle of the original beams; the parts near the ends were generally found to be in an uncracked state. The two undamaged end parts were then cut to form the deep beams as shown in Fig. 2.

The detailed information about the deep beams is given in Table 3. For B2T3-1 and B2T3-2, the configurations of the steel bars were different for the two beams along the length but the net spans were the same. As shown in Fig. 2, B2T3-1 included the ver-tical concrete cover at the end of support A, but the vertical con-crete cover at the ends of supports C and D of B2T3-2 was removed. As a result, no concrete cover existed at the ends of B2T3-2. The steel bars in B2T3-2 were symmetrically distributed, including the longitudinal bars and the stirrups. The objective was to check the influence of the distribution of steel bars on the mechanical performance of the deep beams.

The results of the deep beams that were tested in 2010, at the age of 26 years, have been presented in a previous study [17]. Only the results of the deep beams tested in 2012 at the age of 28 years will be fully described in the following sections. Nevertheless, the analysis and discussion on the influence of the corrosion of reinforcement and the span of beams on the mechani-cal performance of the deep beams will refer to all eight beams.

3.2. Mechanical response of the beams

A three-point loading test was carried out on all the deep beams to test their residual mechanical performance. As shown in Fig. 3, the deflection at mid-span was recorded with a linear variable differential transducer (LVDT). The slip of the tension bars was also monitored by four LVDTs located on the ends of the bars.

During the loading process, the mechanical responses of the corroded deep beams were quite different from those of the uncorroded beams and the failure mode of the corroded beams was significantly different from that of the uncorroded beams.

As shown in Fig. 4, the main cracks appeared under the location of the applied load. Their widths increased gradually and the cracks propagated vertically, nearly reaching the top surface of the beam. Finally, the concrete cover in the tension zone delaminated. One of the tension bars failed at the middle of beam B2Cl3-2 and the beam collapsed. For B2Cl3-1, both of the tension bars failed in the mid-span cross-section. The corroded beams appeared to fail in a mode in which the tension bars yielded or even ruptured.

Table 3
Detailed information about the deep beams.

Deep beams	Age (years)	Length (mm)	Net span (mm)	Status
B2Cl3-1	28	1200	1000	Corroded
B2Cl3-2	28	1040	840	Corroded
B2T3-1	28	1020	820	Un-corroded
B2T3-2	28	1020	820	Un-corroded

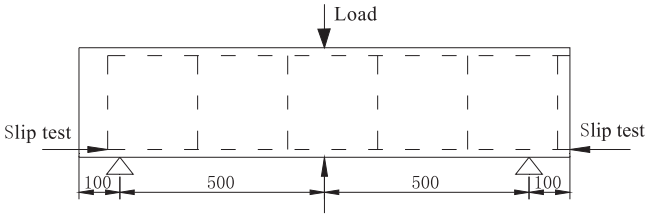

Fig. 3. Typical arrangement of loading test on B2Cl3-1 (mm).

Compared to the corroded beams, the uncorroded beams failed in a more brittle manner. As shown in Fig. 5, several inclined cracks appeared, starting from the tension zones. As the load increased, the cracks gradually extended toward the compressive zone at the top, and the cracks became significantly wider. Finally, the uncorroded beam B2T3-1 failed when the tension bars broke in the tension zone. The failure points of the tension bars were not at the middle of the beam but at the root of the inclined cracks as shown in Fig. 5(a). A stirrup at the root of the inclined crack failed in beam B2T3-2 as shown in Fig. 5(b). In fact, due to the defective concrete cover at the support as shown in Fig. 6, the ten-sion bar near FS-Support C started to slip when the load reached 150 kN. The slip developed as the load increased to about 180 kN. The diagonal crack enlarged significantly, which finally resulted in failure of one stirrup.

3.3. Experimental results of the mechanical tests on the deep beams

Fig. 7 shows the load-deflection curves of both the corroded and uncorroded deep beams. Comparison of the curves indicates that the mechanical response of the deep beams was significantly influenced by corrosion. The capacity was reduced due to corrosion of the reinforcement. However, the ductility of the corroded deep beam B2Cl3-1 was much better than that of the uncorroded beams. This is in agreement with the observation that the reduction of cross-section resulted in the flexural capacity becoming smaller than the shear capacity and the corroded beams failed in a bending failure mode without the inclined cracks. However, the uncorroded deep beams failed in a classic shear failure mode, and there was a significant arch effect in the failure process.

The results for all the deep beams, extracted from the load-deflection curves of Fig. 7, are presented in Table 4. Assuming that the influence of difference in span on the ultimate capacity of the corroded beams was small, the degree of corrosion of the tension bars was studied in order to further identify the mechanical performance of the deep beams.

3.4. Slip of the longitudinal bars

The slip of the tension bars during the loading process on the deep beams was recorded by four LVDTs with an accuracy of 10^{-4} mm. The slip-beam load curves were plotted to show the response of the ends of the tension bars during the whole loading test.

Fig. 8 shows the curves for the corroded beams and Fig. 9 shows the results for the uncorroded beams that were tested in 2012, at the age of 28 years. The support marks A, B, C, and D refer to the ends of the beams as shown in Fig. 2. BS and FS denote the back side and front side tension bars of the deep beam. For example, the legend BS Support A means the slip of the rear tension bar at the location near support A.

According to Figs. 8 and 9, there was almost no slip for either the corroded beams or the uncorroded beams in the loading

(a) Failure of corroded beam B2Cl3-1
(The middle bar visible in this photograph is part of a lifting hook and does not contribute to the strength in bending)

(b) Failure of corroded beam B2Cl3-2 (c) Failure of tension bar of B2Cl3-2

Fig. 4. Typical failure of corroded beams due to the rupture of tension bar at mid-span.

(a) Failure of un-corroded beam B2T3-1 (b) Failure of un-corroded beam B2T3-2

Fig. 5. The typical rupture of deep beams.

process. Slip of the tension bars only occurred when the load reached the ultimate capacity, but the value was still very small even when the deep beams ruptured. This observation supports the conclusion that the anchorage bond between the tension bars and concrete in the support zone was still strong enough to support composite action even though the beams were highly corroded and spalling had occurred in some zones of the concrete cover.

However, it should be pointed out that the slip of front side tension bar near support C of B2T3-2 was larger than that of other results. This may have been due to the damage of the concrete cover near support C when the deep beam was formed, as shown in Fig. 6.

3.5. Corrosion distribution in the corroded bars

The corroded tension bars were extracted from the beams. Corrosion products were cleaned from the residual reinforcement using Clarke's solution [20] so that the residual steel bar could be investigated more clearly. The distribution of the corrosion on the top and bottom sides of the 12 mm bars was measured care-fully and the corrosion pattern is reproduced graphically in Fig. 10. Both pitting corrosion and general corrosion are included in the figure.

The corrosion distribution did not appear to follow a pattern. However, it was clear that the corrosion on the lower side of the bottom bars was more serious than that on the top side, which may have been due to the thinner cover of the bottom surface of the tension bars. Moreover, the failure points that occurred during the mechanical tests were always at the location of pitting corrosion at both the top and bottom of a bar in the middle section of the deep beams. Therefore pitting corrosion played an important role in the mechanical performance of the corroded deep beams.

3.6. Cross-section loss of the tension bars

In order to measure the gravimetric cross-sectional loss of the corroded tension bars, the bars were cut into short lengths over

Fig. 6. Damage to FS support C of B2T3-2.

which the pattern of corrosion was uniform. So the lengths varied depending on the nature of the corrosion distribution along the bar. The aim was to make sure that the corrosion distribution was as constant as possible in each short length. The gravimetric cross-sectional loss of the tension bars was deduced from the steel material properties as described by Zhu et al. [17].

Fig. 11 shows the gravimetric cross-sectional loss of the tension bars along the length of the beams in B2Cl3-1 and B2Cl3-2. The corrosion loss was irregular as was the corrosion distribution, which is shown in Fig. 10. The maximum cross-sectional loss reached 66 mm^2, which was about 59% of the original steel bar. As the corroded deep beams failed at the location of maximum cross-sectional loss in the tension bars, the residual cross-section at this location was used to deduce the load bearing capacity of the corroded beams, as explained in the next section.

A further conclusion that can be drawn from the cross-sectional loss curves is that the cross-sectional loss of the longitudinal bars at the location of the stirrups was usually smaller than in the zones between the stirrups, which could suggest that the stirrups protected the tension bars from corrosion to a certain degree. The reason might be due to the fact that the stirrups were located in front of the load-induced cracks and then exposed to first macrocell corrosion during corrosion initiation. In this case the stirrup acts as anode and the most active cathodic zone is close to the anode and then is the tensile bars connected to stirrups. Even when corrosion turns to microcell due to the development of corrosion-induced cracks, the lower corrosion damage remains close to stirrups.

4. Discussion

The mechanical properties of the corroded bars were discussed in a previous study [16,21,22]. The average results of the tension tests on the tension bars taken from beams B2Cl3 and B2T3 were used to calculate the yield capacity and ultimate capacity of the deep beams. Based on the previous research work, the yield strength of the corroded tension bars was considered to be 560 MPa and the ultimate strength of the corroded bars was 770 MPa. For the uncorroded bars, the yield strength and ultimate strength were 560 MPa and 620 MPa respectively. It should be noted that the ultimate strength of the corroded bars was higher than that of uncorroded bars. The reason could be interpreted as follow: for the corroded bars, the ultimate strength was calculated using the residual cross-section. Indeed, in the tension test, the corroded bars showed a brittle behavior without necking effect of the cross-section. As a result, the residual cross-section mea-sured after the failure corresponded to the actual cross-section and led to an accurate calculation of both yielding and ultimate strength. But for the uncorroded bars, the ultimate strength was calculated using the nominal cross-section. Indeed, in the tension test, the control bars showed a ductile behavior with a significant necking effect of the cross-section at failure location. The actual ultimate strength must be calculated using the actual cross-section taking into account the necking effect, but in design standards the ultimate strength of steel bars was always described using the nominal cross-section, then this definition was adopted in the fol-lowing calculation.

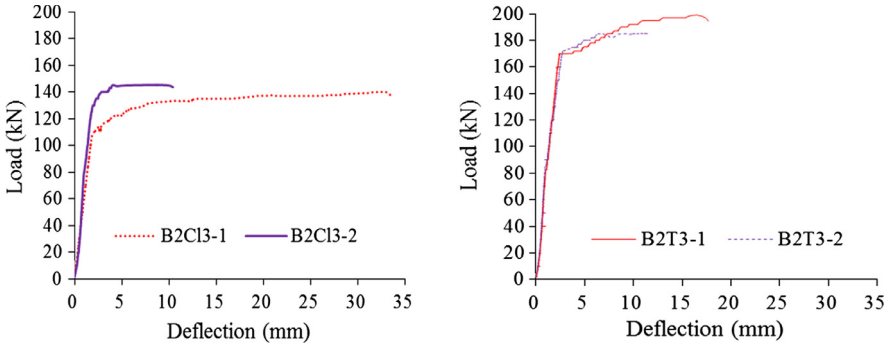

(a) Results of corroded deep beams (b) Results of un-corroded deep beams

Fig. 7. Mechanical performance of the deep beams.

Table 4
Results of the mechanical experiments on the deep beams.

Label	Net span (mm)	Yield capacity (kN)	Ultimate capacity (kN)	Deflection (mm)	Stiffness (kN/mm)	Failure mode
B2Cl3-1	1000	113.8	140.2	33.3	47	Bending
B2Cl3-2	840	140.1	145.3	10.16	68	Bending
B2T3-1	820	170.1	199.0	16.6	71	Shear
B2T3-2	820	172.3	185.1	11.4	63	Shear

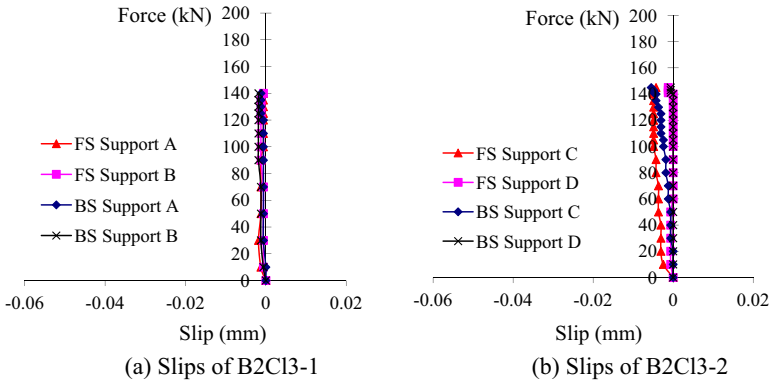

Fig. 8. Slips of tension bars of the corroded beams tested in 2012 (28 years old).

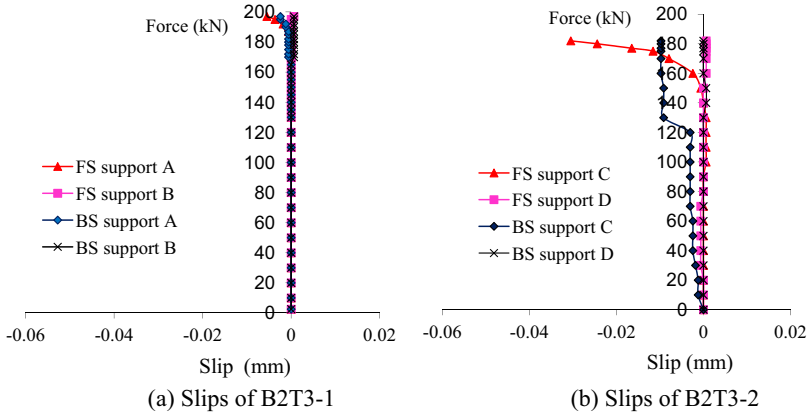

Fig. 9. Slips of tension bars of the un-corroded beams tested in 2012 (28 years old).

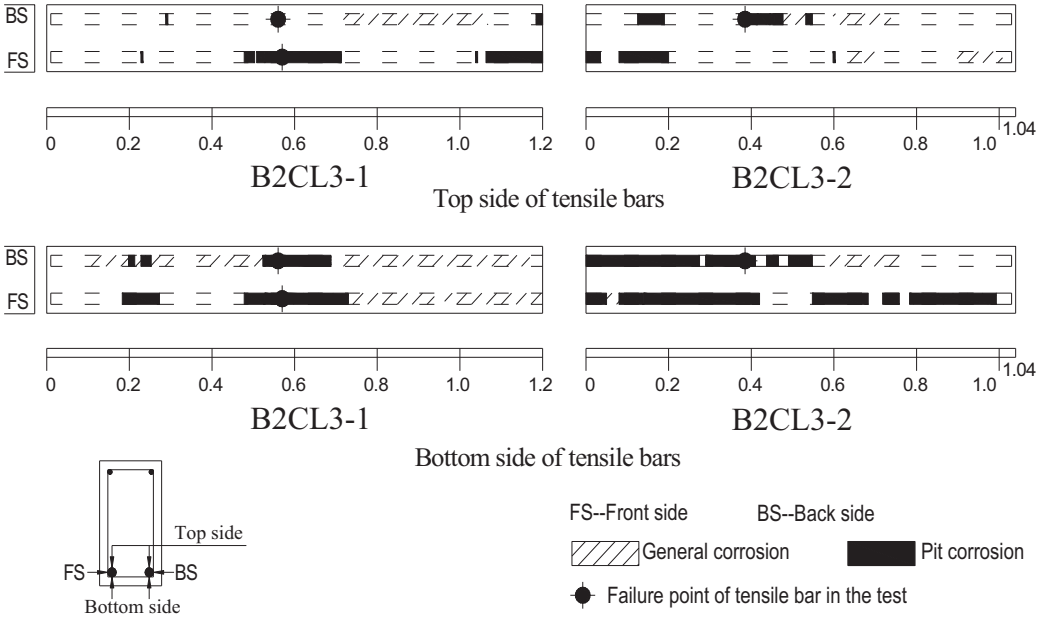

Fig. 10. Corrosion distribution of 28-year-old longitudinal bars.

The ultimate strength of uncorroded steel bar calculated from nominal cross-section was inferior to the actual ultimate strength of corroded bars calculated from actual cross-section. It was probable that the ultimate strength of uncorroded steel appeared to be the same as the one of corroded steel in the actual cross-section after necking was used.

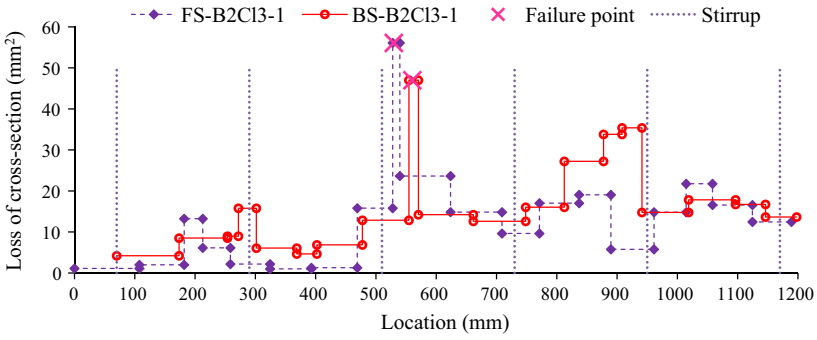

(a) Cross-section loss of tension bars in B2Cl3-1 (28 years)

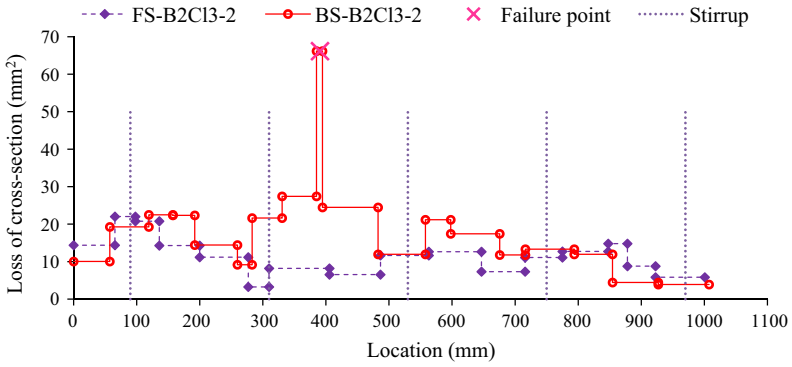

(b) Cross-section loss of tension bars in B2Cl3-2 (28 years)

Fig. 11. Typical cross-section loss of tension bars in deep beams.

Moreover, the ductility of the corroded bars was also studied in this experimental test. The ductility of the reinforcement was strongly influenced by the corrosion. All the research done in this field found that corrosion resulted in a relatively modest change of strength but a significant loss of ductility [28,29]. Castel et al.[23] have proposed a model to predict the ultimate strain of cor-roded bars by using the loss of cross-section. As a result, this loss of ductility could lead to brittle failure of corroded RC beams in flexure.

4.1. Analytical models

As the corroded beams and uncorroded beams had different failure modes, the ultimate capacity of all the deep beams was deduced in different ways based on the experimental response in the mechanical tests. With respect to the bending capacity, the load at reinforcement yield (yield capacity) and at reinforcement rupture (ultimate capacity) were predicted by classical bending theory based on Eurocode 2 [18]. For shear capacity, different shear models were considered, including the Eurocode 2 approach for concrete shear strength, the strut and tie model and the arch effect model. The strut and tie model and arch effect model are described in this section.

According to Eurocode 2, the strut and tie model may be used to predict the shear capacity of deep beams. Based on the experimental performance of the deep beams, the strut and tie model of the deep beams in this programme was defined as in Fig. 12. The strut representing compressive stress fields was formed by the inclined diagonal cracks during the structural response. The ties corresponded to the tension reinforcement and the stirrups across the diagonal cracks.

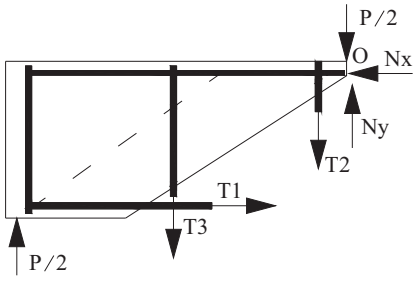

Fig. 12. Strut and tie model of the short beams.

By moment equilibrium about the loading point O, the force P applied to the beam is given by:

$$P = 2 \times \frac{f_{su1} \times l_1 \times A_{sres} + \sum_{i=1}^{2} f_{sui} \times l_i \times A_{swi}}{l_0} \quad (1)$$

The arch effect was also proposed to predict the mechanical capacity of the deep beams [24]. The arch effect model is shown in Fig. 13. Except for un-corroded deep beam B2T3-2, which failed by the failure of the stirrup and the anchorage of the tension bar, all other deep beams in this investigation failed due to failure of the tension bars, and the capacity of deep beams was considered to depend on the longitudinal steel reinforcement. As a result, the capacity P of the deep beams could be deduced by the following equations:

$$P = 2 \times A_{sres} \times f \times \tan\theta \quad (2)$$

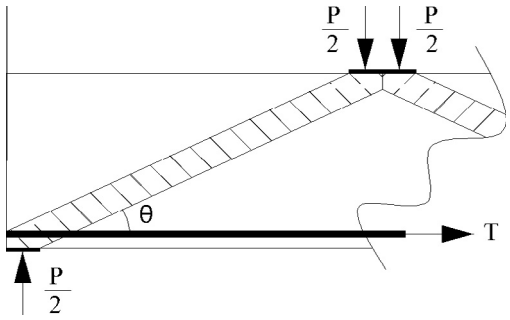

Fig. 13. Arch effect model of the short beams in failure process.

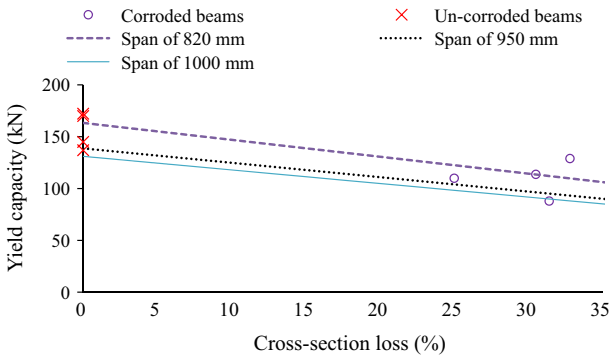

Fig. 14. Influence of corrosion on yield capacity of corroded deep beams by bending theory.

4.2. Comparison of experimental failure loads and predicted load capacities

The cross-section loss of the corroded tension bars was drawn from Fig. 11. The theoretical yield capacity of the deep beams was deduced in different ways. The theoretical results for all the deep beams are shown in Table 5, including the results of speci-mens B2Cl2 and B2T2 [17]. The theoretical results varied signifi-cantly from one to another because of the different theories used. The value closest to experimental results was considered as the theoretical capacity for the deep beams.

As can be seen in Table 5, the results predicted with the arch effect matched the experimental yield capacity for all the uncorroded deep beams. Moreover, the results predicted with the conventional cross-sectional shear calculation also matched the experimental results of B2T2-1 and B2T2-2, which showed that the failure mode of the deep beams was transferred from the arch effect to a combination between bending and shear when the span increased.

The influence of corrosion degree on the yield capacity of deep beams is shown in Fig. 14. As the yield capacities of the corroded deep beams were predicted by bending theory, the trend lines of the theoretical results for the corroded deep beams with different spans are shown in the figure. The residual yield capacity of the deep beams decreased linearly with respect to increasing corrosion degree.

The influence of span on the yield capacity of the uncorroded and corroded (with a corrosion degree of 30% for the tension bars) deep beams based on different models is shown in Fig. 15. The span had no influence on the yield capacity of the deep beams predicted by cross-sectional shear theory. However, the span influenced the yield capacity significantly in the other prediction models. When the span increased, the yield capacity decreased in a non-linear way for both corroded and uncorroded beams.

According to Fig. 15, the strut and tie model overestimated the yield capacity for both the corroded and uncorroded beams. The values predicted by cross-sectional shear theory matched the experimental results well for uncorroded beams, which had a different failure mechanism from the corroded deep beams.

Fig. 15 shows that both the arch effect and bending theory could be applicable to the corroded deep beams and uncorroded deep beams. When the span was over 800 mm, the results predicted by the arch effect model and classical bending theory were very close to each other, which could be a sign of a transition between failure modes. Moreover, the cross-sectional shear capacity of uncorroded beams was close to that of the arch effect. The failure mode transition could be considered to occur for spans between 800 mm and 950 mm in the uncorroded deep beams, in good agreement with Table 5.

The ultimate capacity of all the deep beams was also evaluated using different theories. The theoretical results are shown in Table 6.

The failure loads of corroded deep beams were predicted by bending theory. However, it should be noted that, although the corroded beams showed the same bending failure mode, the ultimate mid-span deflection was quite different. As shown in Fig. 7, the deflection of corroded beam B2Cl3-2 was only 10.16 mm, much less than that of B2Cl3-1 with the value of 33.3 mm. The reason could be that the corroded beam B2Cl3-2 failed because of the brittle properties of the corroded tension bar. The failure points of the tension bars were checked carefully and it was found that there was significant pitting corrosion in the area of the failure point of B2Cl3-2, while more uniform corrosion shape was observed at the failure points of B2Cl3-1. According to previous research [17], the asymmetrical distribution of residual cross-section of the reinforcement was associated with more brittle performance than that of the reinforcement with uniform corrosion even though the corrosion degree was the same.

The uncorroded deep beams failed in shear failure mode. As shown in the table, the prediction using concrete shear strength

Table 5
Comparison of the yield capacity of the deep beams based on different theories.

Label	ΔAs (%)	Span (mm)	P_E (kN)	Different theoretical results (kN)				P_T (kN)	P_T/P_E	Predicted failure mode
				Bending	CS	S&T	Arch			
B2Cl2-1	31.4	950	88.0	100.0	135.8	93.2	103.9	100.0	1.14	Bending
B2Cl2-2	25.0	950	110.0	109.1	138.1	151.2	113.6	109.1	0.99	Bending
B2T2-1	0	950	137.0	133.8	152.6	182.2	151.4	151.4/152.6	1.11/1.11	Arch/CS
B2T2-2	0	950	145.0	144.4	152.6	182.2	151.4	151.4/152.6	1.11/1.05	Arch/CS
B2Cl3-1	30.5	1000	113.8	95.8	136.1	90.1	98.2	95.8	0.84	Bending
B2Cl3-2	32.8	840	129.0	111.8	135.2	103.6	121.2	111.8	0.87	Bending
B2T3-1	0	820	170.0	169.5	152.6	192.1	187.3	187.3	1.10	Arch effect
B2T3-2	0	820	172.3	169.5	152.6	192.1	187.3	187.3	1.09	Arch effect

CS: cross-sectional shear; S&T: Strut and tie model; P_E: experimental results; P_T: theoretical capacity.

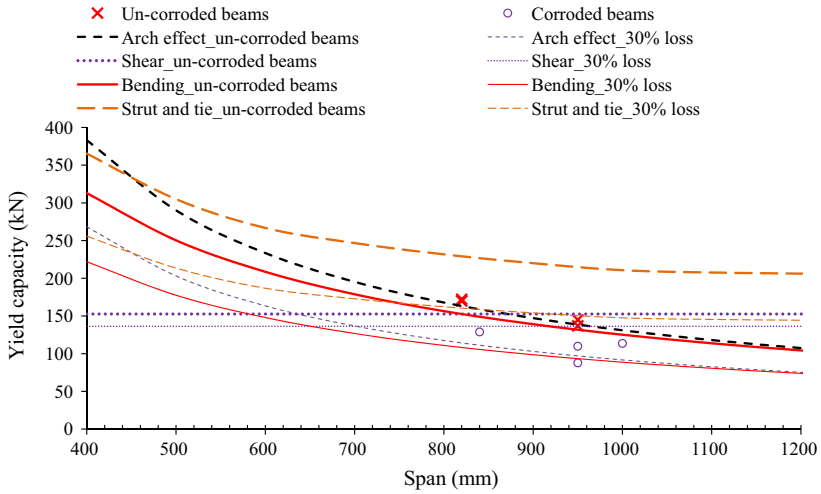

Fig. 15. Influence of different factors on yield capacity of deep beams.

Table 6
Comparison of the ultimate capacity of the deep beams based on different theories.

Label	ΔAs (%)	Span (mm)	P_E (kN)	Different theoretical results (kN)				P_T (kN)	P_T/P_E	Predicted failure mode
				Bending	CS	S&T	Arch			
B2Cl2-1	31.4	950	123.0	136.5	158.4	128.2	142.9	136.5	1.11	Bending
B2Cl2-2	25.0	950	148.0	148.8	160.6	200.1	156.1	148.8	1.01	Bending
B2T2-1	0	950	138.0	147.7	159.7	200.9	167.7	159.7	1.16	CS
B2T2-2	0	950	159.0	159.4	159.7	200.9	167.7	159.7	1.01	CS
B2Cl3-1	30.5	1000	140.0	130.8	158.7	123.9	135.0	130.8	0.93	Bending
B2Cl3-2	32.8	840	145.2	152.7	157.8	142.4	166.7	152.7	1.05	Bending
B2T3-1	0	820	199.0	187.1	159.7	212.6	207.4	207.4	1.04	Arch effect
B2T3-2	0	820	185.0	187.1	159.7	212.6	207.4	207.4	1.12	Arch effect

CS: cross-sectional shear; S&T: Strut and tie model; P_E: experimental results; P_T: net theoretical capacity.

(Eurocode 2) was closest to the experimental failure load for the deep beams with spans of 950 mm while, for the deep beams with spans of 820 mm, the arch theory was closest. This shows that, at a span of about 900 mm, the different theories give similar values but which still depended on the span.

The ultimate capacities of B2T3-1 and B2T3-2 were also quite close to each other. In fact, the net span of the two beams was the same but the reinforcement layout was different. As shown in Fig. 2, the transverse steel configuration of B2T3-1 was asym-metrical, while the transverse steel configuration of B2T3-2 was symmetrical, but with an anchorage defect at one end. B2T3-1 showed shear failure mode with two tension bars failing at the end of the inclined cracks. Failure of B2T3-2 was initiated by the rupture of one stirrup and then followed by slipping of the tension bars with damage to the concrete cover at the end. Finally, the beam collapsed.

The ultimate capacities of the corroded beams were predicted by bending theory. The impact of degree of corrosion on the ultimate capacity for different spans is shown in Fig. 16. The theoretical results showed that the ultimate capacity of the corroded beams decreased in a linear manner with increasing cross-sectional loss of the tension bars.

The theoretical results of the impact of spans with different cross-sectional losses are shown in Fig. 17. The corroded beams were predicted using a corrosion degree of 30% in the two tension bars.

As shown in Fig. 17, the results predicted by the strut and tie model were higher than the experimental results for both corroded and uncorroded deep beams. The cross-sectional shear theory

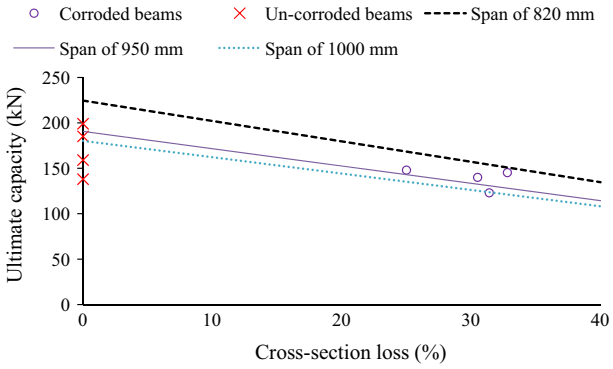

Fig. 16. Influence of corrosion on ultimate capacity of corroded deep beams predicted by bending theory.

predicted the ultimate capacity of B2T3-1 and B2T3-2 well but with slightly lower results than those found experimentally.

Fig. 17 indicates that the relationship between the predicted ultimate capacity of the deep beams and their span was non-linear except for the cross-sectional shear values. It was clear that the ultimate capacity decreased when the span increased for both the corroded and uncorroded beams. With the increase in span, the results predicted by bending theory gradually came closer to those from the arch effect and the failure mode of uncorroded deep beams gradually changed from the arch effect to cross-sectional shear as the span increased to 950 mm.

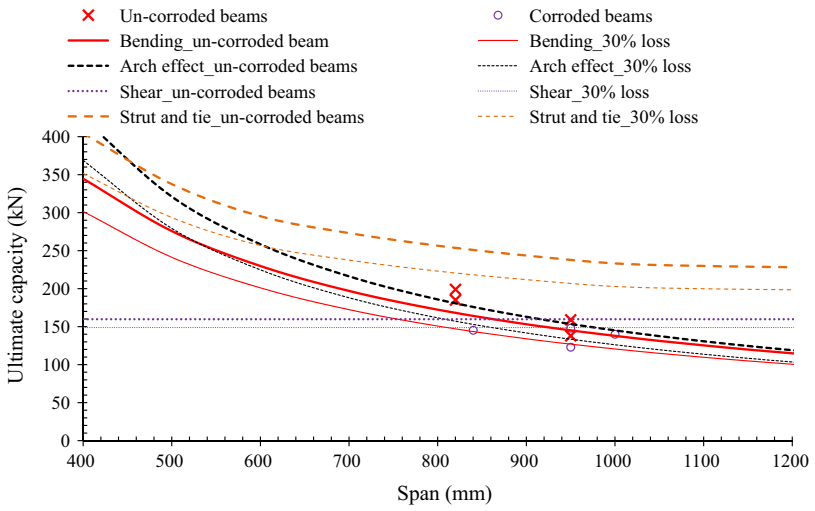

Fig. 17. Influence of different factors on ultimate capacity of deep beams.

It is interesting to note that the experimental results showed that the corroded deep beams failed in bending failure mode as shown in Table 6 but that the values predicted by bending theory and arch effect were both close to the experimental results, which showed the transition of the failure mode from arch effect to bending. Moreover, the transition zone of the span for the corroded deep beams became smaller than that of the un-corroded beams. For un-corroded beams, the failure mode changed from flexure to shear at a span of 1100 mm while the change occurred at a lower span of 800 mm for beams with 30% corrosion.

4.3. Anchorage of the tension bars

The slipping of the tension bars indicates that the anchorage bond strength of the bars in the residual concrete was not exceeded [25]. Based on Model Code 2000 [26], Al-Mahmoud et al. [27] proposed an Eq. (3) to deduce the anchorage strength of uncorroded tension bars. The results are shown in Table 7.

$$\tau_u = \frac{\sigma_{(\max)} \cdot A}{\Sigma \cdot L_{\text{anch}}} \cdot \frac{1+\alpha}{1-\alpha} \tag{3}$$

where α is a curve-fitting parameter proposed by Al-Mahmoud et al. [27] that influences the shape of the bond-slip curve in the ascending branch and is obtained by equating the area underneath the ascending branch of the experimental curve to the value. In this investigation, there were no hooks at the ends of the tension bars. So, the transmission length of 15 times the diameter of tension bars (180 mm) was taken as the anchorage length for the undamaged beams [18].

However, for the damaged uncorroded beam (Fig. 6) and corroded beams, a new parameter was proposed to consider the effect of the reduction of corrosion on the bond strength, giving the following improved equation:

$$\tau_u = \frac{\sigma_{(\max)} \cdot A}{\gamma \cdot \Sigma \cdot L_{\text{anch}}} \cdot \frac{1+\alpha}{1-\alpha} \tag{4}$$

For the non-spalling bars of corroded beams, γ was assumed to be 0.8 and, for the anchorage with spalling zone, 0.6 was taken. The anchorage length of the corroded or damaged zone was considered to be 20 times the diameter of the tension bars (240 mm).

It should be noted that the ultimate stress remained the same when the anchorage length was larger than the transmission length according to the research of Al-Mahmoud et al. [27]. So, in the following calculation, the transmission length of the corroded and uncorroded deep beams in non-spalling and undamaged anchorage zones had the same value.

Al-Mahmoud et al. [27] found that the peak bond strength was about 10 MPa but the influence of the support pressure and the

Table 7
Anchorage of the tension bars at the ends of all the beams.

Beam	Location	L_{anch} (mm)	γ	τ_u (MPa)	Slip state	Location	L_{anch} (mm)	γ	τ_u (MPa)	Slip state
B2Cl2-1	A-FS	240	0.8	8.42	No	B-FS	240	0.6	11.22	Occurred
	A-BS	240	0.8	8.42	No	B-BS	240	0.6	11.22	Occurred
B2Cl2-2	C-FS	240	0.8	8.42	No	D-FS	240	0.8	8.42	No
	C-BS	240	0.8	8.42	No	D-BS	240	0.8	8.42	No
B2T2-1	A-FS	180	1.0	10.33	Initiation	B-FS	180	1.0	10.33	Initiation
	A-BS	180	1.0	10.33	Initiation	B-BS	180	1.0	10.33	Initiation
B2T2-2	C-FS	180	1.0	10.33	Initiation	D-FS	180	1.0	10.33	Initiation
	C-BS	180	1.0	10.33	Initiation	D-BS	180	1.0	10.33	Initiation
B2Cl3-1	A-FS	240	0.8	8.42	No	B-FS	240	0.8	8.42	No
	A-BS	240	0.8	8.42	No	B-BS	240	0.8	8.42	No
B2Cl3-2	C-FS	240	0.8	8.42	No	D-FS	240	0.8	8.42	No
	C-BS	240	0.8	8.42	No	D-BS	240	0.8	8.42	No
B2T3-2	A-FS	180	1.0	10.33	Initiation	B-FS	180	1.0	10.33	Initiation
	A-BS	180	1.0	10.33	Initiation	B-BS	180	1.0	10.33	Initiation
B2T3-2	C-FS	240	0.6	12.92	Occurred	D-FS	180	1.0	10.33	Initiation
	C-BS	180	1.0	10.33	Initiation	D-BS	180	1.0	10.33	Initiation

Locations A, B, C and D are shown in Fig. 2 FS: front side tension bar; BS: back side tension bar.

presence of the stirrups was not considered in their model. So the peak value would be higher for the beams in this paper. As a result, 10 MPa was treated as the initiation of the slip, which could match the experimental results as shown in Figs. 8 and 9. For the corroded deep beams, the bond stresses of B-FS and B-BS of B2Cl1-1 were above this value and slight slip therefore occurred at these ends. But for the other points of the corroded deep beams, the bond stresses were still under this criterion and no slips were found in these zones, as shown in Fig. 8 and in the literature [15]. For the uncorroded deep beams, the bond strength of C-FS of B2T3-2 was 12.92 MPa, which could explain the slip of the tension bars in Fig. 9. However, the bond strength of most of the undamaged uncorroded deep beams was around the criterion, which agrees well with the experimental results that most of the recorded values showed signs of slips as recorded in Fig. 9.

5. Conclusion

Based on the experimental tests on four long-term chloride corroded deep beams and four uncorroded deep beams, the mechanical performance of deep beams has been presented in this paper. The corroded beams were stored in a chloride environment which was close to natural corrosion conditions. The following conclusions can be drawn:

(1) The mechanical performance of the deep beams was changed by corrosion. When the net span was the same, the corroded beams showed bending failure, while the uncorroded beams showed shear failure (arch effect).
(2) The ductility of the deep beams was not reduced by corrosion because of the change in failure mode for the corroded beams. The uncorroded beams were rather brittle and the beams failed in shear. In contrast, the deflection of the corroded beams increased considerably due to their bending failure instead of shear failure.
(3) With the increase in span, the value predicted by the arch effect model gradually came close to bending theory. For the corroded deep beams, the transition between failure modes occurred at shorter spans than in uncorroded beams.
(4) Despite the corrosion spalling at the anchorage, the bond strength of the tension bars was not reduced and did not correspond to a weak point for the behavior of corroded deep beams. In contrast, the accidental spalling of concrete at the anchorage of the FS bar near support C of the control beam led to bar slip during the yielding plateau and finally to the failure of the deep control beam.

Acknowledgement

The first author gratefully acknowledges the financial support of the Fundamental Research Funds for the Central Universities under Grant KCRC14007536.

References

[1] Azad AK, Ahmad S, Azher SA. Residual strength of corrosion-damaged reinforced concrete beams. ACI Mater J 2007;104(1):40–7.
[2] Auyeung Y, Balaguru P, Chung L. Bond behavior of corroded reinforcement bars. ACI Mater J 2000;97(2):214–20.
[3] Coronelli D, Gambarova P. Structural assessment of corroded reinforced concrete beams: modeling guidelines. J Struct Eng 2004;130(8):1214–24.
[4] Cabrera JG. Deterioration of concrete due to reinforcement steel corrosion. Cem Concr Compos 1996;18(1):47–59.
[5] Mangat PS, Elgarf MS. Flexural strength of concrete beams with corroding reinforcement. ACI Struct J 1999;96(1).
[6] Malumbela G, Alexander M, Moyo P. Variation of steel loss and its effect on the ultimate flexural capacity of RC beams corroded and repaired under load. Constr Build Mater 2010;24(6):1051–9.
[7] Torres-Acosta AA, Navarro-Gutierrez S, Terán-Guillén J. Residual flexure capacity of corroded reinforced concrete beams. Eng Struct 2007;29(6): 1145–52.
[8] Xia J, Jin W, Li L. Shear performance of reinforced concrete beams with corroded stirrups in chloride environment. Corros Sci 2011;53(5):1794–805.
[9] Cairns J. Strength in shear of concrete beams with exposed reinforcement. Proc ICE-Struct Build 1995;110(2):176–85.
[10] Higgins C, Farrow III WC. Tests of reinforced concrete beams with corrosion-damaged stirrups. ACI Struct J 2006;103(1).
[11] Rodriguez J, Ortega LM, Casal J. Load carrying capacity of concrete structures with corroded reinforcement. Constr Build Mater 1997;11(4):239–48.
[12] Yuan Y, Ji Y, Shah SP. Comparison of two accelerated corrosion techniques for concrete structures. ACI Struct J 2007;104(3):344–7.
[13] François R, Arliguie G. Influence of service cracking on reinforcement steel corrosion. J Mater Civ Eng 1998;10(1):14–20.
[14] Zhu WJ, François R. Corrosion of the reinforcement and its influence on the residual structural performance of a 26-year-old corroded RC beam. Constr Build Mater 2014;51:461–72.
[15] Vidal T, Castel A, François R. Corrosion process and structural performance of a 17 year old reinforced concrete beam stored in chloride environment. Cem Concr Res 2007;37:1551–61.
[16] Zhu WJ, François R. Effect of corrosion pattern on the ductility of tensile reinforcement extracted from a 26-year-old corroded beam. Adv Concr Constr 2013;1(2):121–37.
[17] Zhu WJ, François R, Coronelli D, Cleland D. Effect of corrosion of reinforcement on the mechanical behaviour of highly corroded RC beams. Eng Struct 2013;56:544–54.
[18] CEN, Eurocode 2: Design of concrete structures. Part 1–1: General rules and rules for buildings. British Standards Institution; 2004.
[19] Zhu WJ, François R. Prediction of the residual load-bearing capacity of naturally corroded beams using the variability of tension behaviour of corroded steel bars. Structure and Infrastructure Engineering: Maintenance, Management, Life-Cycle Design and Performance; 2015. http://dx.doi.org/10.1080/15732479.2014.996165.
[20] A. G1-03. Standard practice for preparing, cleaning, and evaluating corrosion test specimens; 2003.
[21] Zhu WJ, François R. Structural performance of RC beams corroded in chloride environment for a long period. Mater Struct 2014. http://dx.doi.org/10.1617/s11527-014-0270-2.
[22] Zhu WJ, François R. Experimental investigation of the relationships between residual cross-section shapes and the ductility of corroded bars. Constr Build Mater 2014;69:335–45.
[23] Castel R, François R, Arliguie G. Mechanical behavior of corroded reinforced concrete beams-part 2: bond and notch effects. Mater Struct 2000;33(9): 545–51.
[24] Spinella N. Shear strength of full-scale steel fibre-reinforced concrete beams without stirrups. Comput Concr 2013;11(5):365–82.
[25] Al-Mahmoud F, Castel A, François R, Tourneur C. Effect of surface pre-conditioning on bond of carbon fibre reinforced polymer rods to concrete. Cem Concr Compos 2007;29(9):677–89.
[26] fib Bulletin 55: Model Code 2010, First complete draft-volume 1.
[27] Al-Mahmoud F, Castel A, François R. Failure modes and failure mechanisms of RC members strengthened by NSM CFRP composites–analysis of pull-out failure mode. Compos Part B Eng 2012;43(4):1893–901.
[28] Apostolopoulos CA, Koutsoukos PG. Study of the corrosion of reinforcement in concrete elements used for the repair of monuments. Constr Build Mater 2008;22:1583–93. http://dx.doi.org/10.1016/j.conbuildmat.2007.03.022.
[29] Apostolopoulos CA, Papadopoulos MP, Pantelakis SG. Tensile behavior of corroded reinforcing steel bars BSt 500s. Constr Build Mater 2006;20:782–9. http://dx.doi.org/10.1016/j.conbuildmat.2005.01.065.